J Biomol NMR (2013) 55:11–17
DOI 10.1007/s10858-012-9692-8

COMMUNICATION

Residue-specific membrane location of peptides and proteins using specifically and extensively deuterated lipids and ^{13}C–^{2}H rotational-echo double-resonance solid-state NMR

Li Xie · Ujjayini Ghosh · Scott D. Schmick · David P. Weliky

Received: 16 October 2012 / Accepted: 28 November 2012 / Published online: 8 December 2012

Abstract Residue-specific location of peptides in the hydrophobic core of membranes was examined using ^{13}C–^{2}H REDOR and samples in which the lipids were selectively deuterated. The transmembrane topology of the KALP peptide was validated with this approach with substantial dephasing observed for deuteration in the bilayer center and reduced or no dephasing for deuteration closer to the headgroups. Insertion of β sheet HIV and helical and β sheet influenza virus fusion peptides into the hydrophobic core of the membrane was validated in samples with extensively deuterated lipids.

Keywords REDOR · Membrane location · Deuterated lipid · Solid-state NMR · Peptide · Protein · ^{13}C–^{2}H

For membrane peptides and proteins, one significant contribution of magic angle spinning (MAS) solid-state NMR is the determination of high-resolution structure in intact membranes with a lipid and/or sterol composition close to that of the cell membrane (Yang et al. 2001; McDermott 2009). For some of these peptides and proteins, residue-specific membrane location is critical to function. Some examples include antimicrobial peptides and the fusion peptide region of viral fusion proteins (Doherty et al. 2006; Qiang et al. 2009; Pan et al. 2010). There has been some development of solid-state NMR methods to determine membrane location including those based on measurement of increased relaxation rate in the presence of paramagnetic species (Buffy et al. 2003). These paramagnetic species may be soluble ions such as Mn^{2+}or lipids derivatized with functional groups that are stable free radicals. Another approach has been measurement of spin diffusion from mobile protons either in water at the membrane surface or in methyl groups at the termini of acyl chains (Huster et al. 2002; Gallagher et al. 2004). Analysis of these rates to determine distances between protein and lipid nuclei can depend on estimation of the spectral density of motions and often only a qualitative model of membrane location is derived from the analysis. These analyses also typically provide an average internuclear parameter (through dipolar coupling) rather than a distribution of parameters and hence distribution of distances.

An alternate solid-state NMR approach has been direct detection of dipolar couplings between specific nuclei in the protein and specific nuclei in the lipid molecules in the membrane. The most common application of this approach has been rotational-echo double-resonance (REDOR) between protein ^{13}C nuclei (or sometimes ^{15}N nuclei) and lipid ^{31}P nuclei (Toke et al. 2004; Doherty et al. 2006; Qiang et al. 2009). REDOR is a widely-applied method to measure heteronuclear dipolar couplings and is relatively insensitive to resonance offsets and pulse imperfections. These couplings are determined by analysis of the ^{13}C spectral intensities (transformed into dephasing $\equiv \Delta S/S_0$) for a set of dephasing times (τ). For non-phosphorylated proteins, analysis of the ^{13}C–^{31}P REDOR provides a distance or a distribution of distances between a specific protein ^{13}C and the ^{31}P layer of the lipid headgroups. For example, analysis of ^{13}C–^{31}P REDOR data for a membrane-associated HIV fusion peptide labeled at a specific backbone ^{13}CO provided the fraction of the peptides (to ± 0.05 precision) with ^{13}CO–^{31}P distance >10 Å (Qiang et al. 2009). For the remaining fraction of more proximal ^{13}CO nuclei, the ^{13}CO–^{31}P distance was determined to ±0.5 Å precision. Combining the fractions and distances

L. Xie · U. Ghosh · S. D. Schmick · D. P. Weliky (✉)
Department of Chemistry, Michigan State University, 578 S. Shaw Lane, East Lansing, MI 48824, USA
e-mail: weliky@chemistry.msu.edu

from samples labeled at different ^{13}CO nuclei provided evidence for insertion of the central apolar region of the peptide into a single membrane leaflet.

There has also been effort to measure distances between peptide ^{13}C nuclei and nuclei in the lipid acyl chains in the membrane interior. Because both the peptide and acyl chains are extensively protonated, ^{13}C–^{1}H REDOR is typically not informative about peptide proximity to these chains. An alternative has been ^{13}C–^{19}F REDOR on samples whose membranes have a small mole fraction (<0.1) of lipids with a ^{1}H → ^{19}F substitution at a single site in the acyl chain (Toke et al. 2004; Qiang et al. 2009). As one specific example, membrane insertion of the HIV fusion peptide was supported by REDOR-detected contact between Ala-6 ^{13}CO and lipid ^{19}F in samples with membranes containing 0.09 mol fraction DPPC-F5 lipid with a ^{1}H → ^{19}F substitution at C5 in the palmitoyl chains of dipalmitoylphosphatidylcholine (DPPC). The ^{13}CO–^{19}F distance was determined up to 10 Å with ±0.5 Å precision. However, the ^{1}H → ^{19}F substituted lipids have some disadvantages. Because the ^{1}H → ^{19}F substitution is a chemical change, the position of the ^{19}F in the membrane might be different than the location of the ^{1}H that it replaces. In addition, interdigitated rather than bilayer phase is formed for samples containing 100 % DPPC-F16 monofluorinated at the terminus of the acyl chain (Hirsh et al. 1998). The maximum lipid mole fraction of fluorinated lipid is therefore ~0.1 (Toke et al. 2004; Qiang et al. 2009). In addition to the intrinsic ^{13}CO–^{19}F distance distribution due to peptide membrane locations, the ^{19}F dilution adds a second distribution of ^{13}CO–^{19}F distances and it is difficult to deconvolve these two distributions. It is additionally problematic that DPPC-F16 is the only commercially available fluorinated lipid. Monofluorinated fatty acid precursors are also not commercially available and custom synthesis is required (Qiang et al. 2009).

To our knowledge, REDOR between peptide/protein ^{13}C nuclei and lipid ^{2}H nuclei is a new approach to probe membrane location (Schmidt et al. 1992). Strengths of this approach include: (1) ^{2}H is chemically equivalent to ^{1}H so any fraction of deuterated lipid can be used in the membrane; (2) ^{2}H has very small 1.5×10^{-4} fractional natural abundance; (3) lipids with extensive deuteration are commercially available, e.g. D54 with perdeuteration of the myristoyl chains, Fig. 1; and (4) fatty acids with more selective deuteration are commercially available and can be synthesized into lipids, e.g. D4, D8, and D10 with selectively labeled palmitoyl chains in Fig. 1. One challenge of ^{13}C–^{2}H REDOR is the ~250 kHz breadth of quadrupolar anisotropy in static segments with consequent ^{2}H pulse resonance offsets as large as 125 kHz. Despite this challenge, ^{13}C–^{2}H REDOR has been developed and applied to determining backbone dihedral angles in silk peptides as well as peptide ^{13}C-ligand ^{2}H distances in the membrane-associated influenza M2 proton channel (Gullion et al. 2003; Cady et al. 2010).

Van der Waals radii support a minimal distance of 4–5 Å between a protein backbone ^{13}C and lipid ^{2}H. We therefore developed our ^{13}C–^{2}H REDOR experiment with a lyophilized "I4-A9$_{C}$A8$_{D}$" peptide (sequence AEAAA KEAAAKEAAAKAW) that is predominantly α helical in its lyophilized form and which was ^{13}CO labeled at A9 and ^{2}H labeled at Hα of A8 (Long and Tycko 1998; Zheng et al. 2006). In regular α helical structure, the ^{13}CO–^{2}H internuclear distance is 5.0 Å with dipolar coupling $d = 37$ Hz. Figure 2b shows ^{13}C REDOR spectra of I4-A9$_{C}$A8$_{D}$. The most prominent feature is the ^{13}CO peak at 178.9 ppm. The A9 ^{13}CO contributes ~0.85 fraction of the ^{13}CO signal and the peak shift is consistent with helical structure at A9 (Zhang et al. 2003).

For the typical ^{13}C–^{2}H REDOR pulse sequence, evolution of ^{13}C transverse magnetization during τ due to the ^{2}H dipolar field is refocused (not refocused) during S_0 (S_1) acquisition with additional ^{2}H pulse(s) in S_1. For rotor period = τ_R and $\tau = n\tau_R$ where n is an even integer, a common REDOR "X" pulse sequence includes ^{13}C π pulses at $\tau_R/2$, τ_R, $3\tau_R/2$,…, $(n-1)\tau_R/2$, $(n+1)\tau_R/2$, $(n+2)\tau_R/2$,…, $(2n-1)\tau_R/2$, i.e. at half- and full-rotor cycle periods except $m\tau_R/2$ and $m\tau_R$ (Gullion et al. 2003; Cady et al. 2010). The S_1 acquisition had an additional ^{2}H π/2 or ^{2}H π pulse at $n\tau_R/2$. Because the maximum resonance offset for ^{13}C is ~5 % of that of ^{2}H in static segments, an advantage of the X sequence is minimization of resonance offset effects. This sequence was tried with I4-A9$_{C}$A8$_{D}$ but the $S_0(\tau = 16$ ms)/$S_0(\tau = 2$ ms) intensity ratio was 0.01 presumably because refocusing of ^{13}C evolution from the ^{13}CO anisotropic shift field was reduced by interference between MAS and the ^{13}C π pulse at the midpoint of the rotor period.

The "XY" REDOR pulse sequence, Fig. 2a, is a variant of a sequence commonly applied to systems in which both nuclei are spin ½. During S_0 and S_1 acquisitions, ^{13}C π pulses are applied at τ_R, $2\tau_R$,…, $(n-1)\tau_R$, i.e. at the end of each rotor period except the last one. During S_1, ^{2}H π pulses are applied at $\tau_R/2$, $3\tau_R/2$,…, $(2n-1)\tau_R/2$, i.e. at the midpoints of each rotor period. For I4-A9$_{C}$A8$_{D}$, the $S_0(\tau = 16$ ms)/$S_0(\tau = 2$ ms) intensity ratio was 0.70. Figure 2b displays a plot of the normalized dephasing versus τ where this $\Delta S/S_0$ dephasing = $(S_0 - S_1)/S_0$ intensity ratio. For $\tau = 40$ ms, $\Delta S/S_0 = 0.54$. The "Y" REDOR pulse sequence was also tried with one ^{13}C π pulse at the midpoint of τ for both S_0 and S_1 and ^{2}H π pulses for S_1 at $\tau_R/2$, τ_R, $3\tau_R/2$,…, $(n-1)\tau_R/2$, $(n+1)\tau_R/2$, $(n+2)\tau_R/2$,…, $(2n-1)\tau_R/2$, i.e. at half-and full-rotor cycle periods except $n\tau_R/2$ and $n\tau_R$ (Sack et al. 2000). For I4-A9$_{C}$A8$_{D}$, the $S_0(\tau = 16$ ms)/$S_0(\tau = 2$ ms) intensity ratio was 0.16 and $\Delta S/S_0 = 0.35$ at $\tau = 40$ ms.

XY REDOR was used for subsequent experiments because it gave the highest signal-to-noise and largest $\Delta S/S_0$.

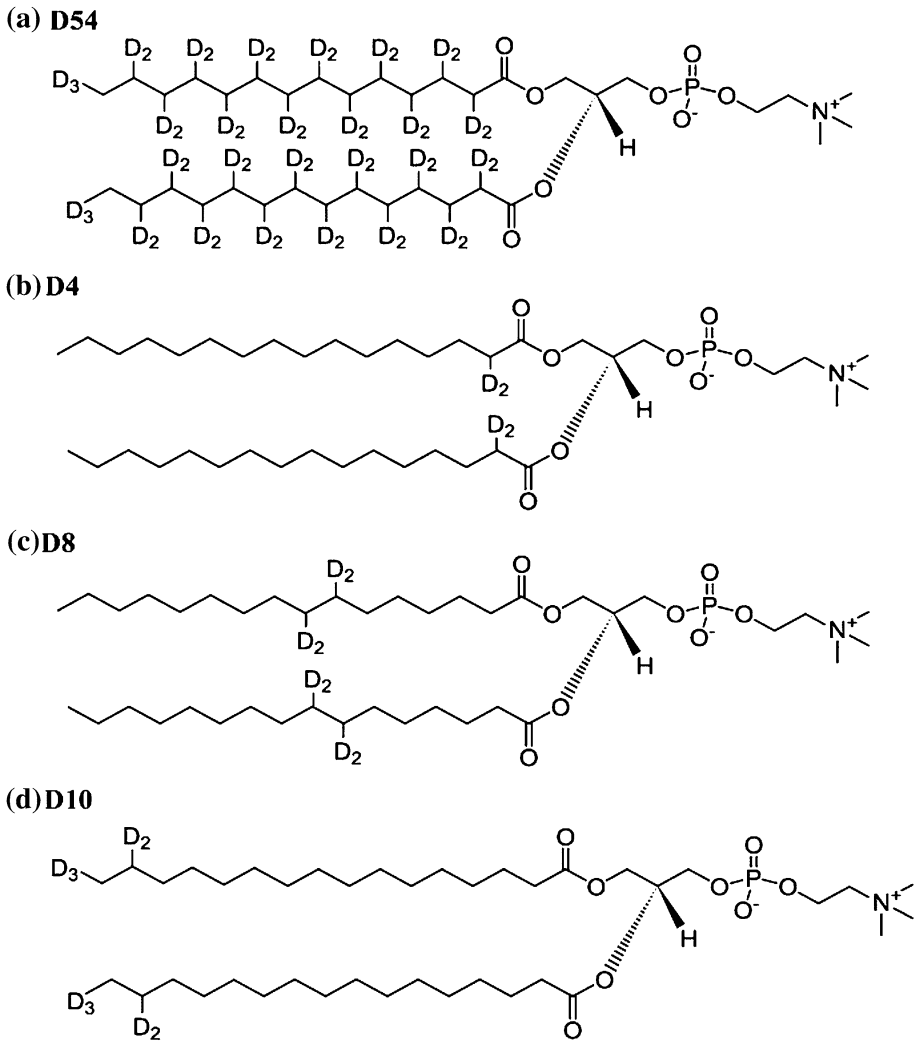

Fig. 1 **a** D54: dimyristoylphosphatidylcholine perdeuterated in the myristoyl chains; **b–d** D4, D8, and D10: dipalmitoylphosphatidylcholine deuterated at palmitoyl carbons 2; 7 and 8; and 15 and 16, respectively. D54 was purchased directly from Avanti Polar Lipids (Alabaster, AL, USA). For D4, D8, and D10, the deuterated palmitic acids were purchased from CDN Isotopes (Pointe Claire, Quebec, Canada) and the lipids were synthesized by Avanti

The ^{1}H and ^{13}C pulse parameters were calibrated as was previously done for ^{13}C–^{15}N REDOR of peptides (Zheng et al. 2006). The ^{2}H field at resonance was ~110 kHz and was calibrated using liquid D_2O and a single pulse sequence without echoes. For I4-A9$_C$A8$_D$, the maximum $\Delta S/S_0$ was achieved with ^{2}H pulses of ~4.3 μs duration which are approximately π pulses. For τ = 64 ms of I4-A9$_C$A8$_D$, $\Delta S/S_0$ reached a value of ~0.58. Half this value was achieved with $\tau_{½} \approx 20$ ms and corresponding $\lambda_{½} = d \times \tau_{½} \approx 0.7$ which is a typical $\lambda_{½}$ value for REDOR between two spin ½ nuclei (Gullion 1998). For the labeled ^{13}CO, a maximum $(\Delta S/S_0)^{max}$ of ~0.68 was calculated using S_0 fractional intensity contributions of 0.85 (0.15) from labeled (natural abundance) ^{13}CO nuclei and no dephasing for most natural abundance ^{13}CO nuclei. This $(\Delta S/S_0)^{max}$ is close to the theoretical value of 2/3 calculated with consideration that a π pulse induces transitions of ^{2}H nuclei in the $m_s = \pm 1$ states but not in the $m_s = 0$ state (Gullion 1999). The ^{2}H pulses in the XY pulse sequence are simple whereas composite ^{2}H pulses have been previously used for the X and Y sequences (Sack et al. 2000; Gullion et al. 2003; Cady et al. 2010). Composite ^{2}H pulses may result in larger $\Delta S/S_0$ and more rapid buildup of $\Delta S/S_0$ with τ. However, comparison was made between Fig. 2b and previous work on a ^{13}CO/^{2}H-labeled peptide with $d = 55$ Hz (Gullion et al. 2003). For this peptide, X REDOR with a composite ^{2}H π/2 pulse produced an asymptotic $\Delta S/S_0$ and $\lambda_{½}$ (≈0.7) that were comparable to the values we obtained with XY REDOR and simple ^{2}H pulses.

Membrane location by ^{13}C–^{2}H REDOR was tested using the "KALP-A11$_C$" designed peptide with sequence GKKLALALALALALALALALKKA, N-terminal acetylation, C-terminal amidation, and a ^{13}CO label at A11 (de Planque et al. 2001). The sequence was designed to traverse the membrane bilayer as a regular α helix. The A11 ^{13}CO is at the midpoint of the apolar L4 to L20 region and would be at the bilayer center in this location model, Fig. 3. Samples were made with KALP-A11$_C$ and either D4, D8, D10 lipid. The KALP-A11$_C$ (1 μmol) and lipid (50 μmol) were first dissolved in a 2:3:2 mixture of 2,2,2-trifluoroethanol,

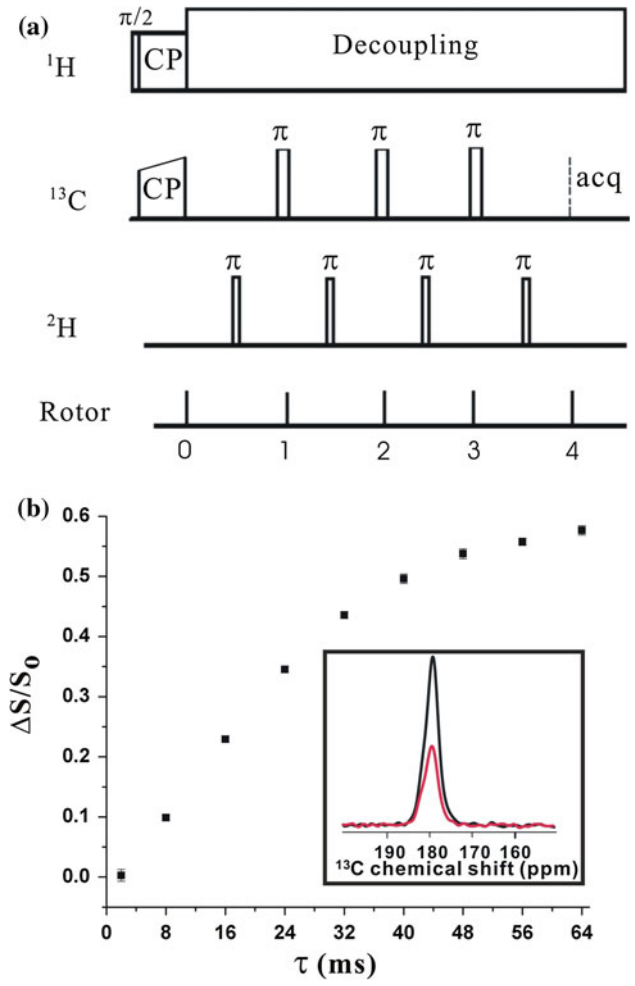

Fig. 2 **a** XY pulse sequence for ^{13}C–^{2}H REDOR with $\tau = 4\tau_R$. The ^{2}H π pulses are absent in the S_0 acquisition and CP ≡ cross-polarization. There was XY-8 phase cycling on the ^{13}C π pulses and XY-8 phase cycling on the ^{2}H π pulses with complete phase cycling during most of the dephasing period except for a typically incomplete last cycle. **b** Plot of $\Delta S/S_0$ versus τ for ~15 μmol of lyophilized I4-A9$_C$A8$_D$ peptide. The S_0 and S_1 intensities were calculated using 1.0 ppm integration range centered at the peak shift. The typical ±σ uncertainty in $\Delta S/S_0$ is approximately the vertical dimension of the square and the calculation of σ used the amplitude of spectral noise (Zheng et al. 2006). *Inset*: S_0 (*black*) and S_1 (*red*) spectra for $\tau = 40$ ms. NMR acquisition conditions included 10.0 kHz MAS frequency, –50 °C cooling gas and ~–30 °C sample temperatures, 5.1 ms acquisition, and 600 scans for each S_0 and each S_1 acquisition. The ^{1}H parameters included 5.0 μs π/2 pulse, 50 kHz CP for 1.7 ms; and 76 kHz decoupling. The ^{13}C parameters included 159.4 ppm transmitter shift, 66–70 kHz CP, and 8.3 μs π pulses. The ^{2}H pulse parameters are discussed in the main text. Processing included 20 Hz Gaussian line broadening and baseline correction

chloroform, and 1,1,1,3,3,3-hexafluoroisopropanol and the solvent was then removed by nitrogen gas and overnight vacuum. The solid was packed in a 4 mm diameter MAS rotor with subsequent addition of 20 μL of buffer (5 mM HEPES/10 mM MES, pH 7.4). The initial organic co-solubilization minimized the fraction of kinetically trapped

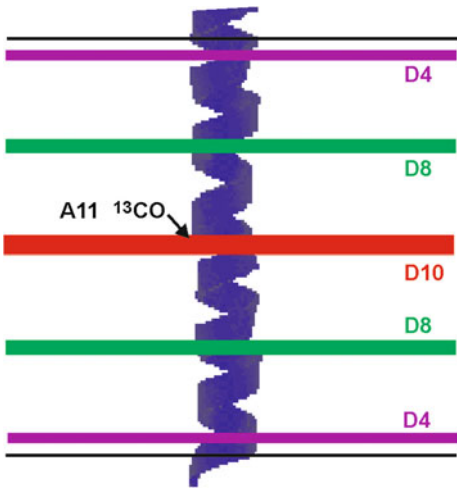

Fig. 3 Model for membrane location of KALP-A11$_C$. The two black lines represent the extrema of the ~31 Å thickness of the palmitoyl chains in the likely subgel phase state of DPPC (Tristram-Nagle and Nagle 2004). The shaded areas represent the approximate longitudinal locations of the deuterons in the D4, D8, and D10 samples with 1, 1.5, and 2 Å thicknesses, respectively. The locations are based on fully extended and tilted chains in the subgel phase and for D8 and D10, the thicknesses are based on the multiple carbon sites which are deuterated. The KALP-A11$_C$ is modeled as a regular α helix centered in the bilayer with parallel helix and bilayer normal axes. The most hydrophobic L4 to L20 region traverses ~25Å along the bilayer normal and the A11 ^{13}CO is at the approximate midpoint of the palmitoyl region

KALP-A11$_C$ on the membrane surface. Solid-state NMR experiments were done with an Agilent 9.4 T spectrometer and T3 triple resonance probe with NMR parameters listed in the Fig. 2 caption.

The ^{2}H spectra of static D4, D8, and D10 samples at ~–30 °C were measured using the solid-echo sequence, i.e. $(\pi/2)_x$-τ-$(\pi/2)_y$-τ-acquire. For all samples, there were approximately symmetric quadrupolar powder patterns centered about the transmitter frequency. For the D4 and D8 samples, the highest intensity "horns" in the patterns were at ~58 kHz which is very close to the ~60 kHz value expected for ^{2}H in immobile –CD_2– groups. The D10 sample had horns at both ~60 and ~15 kHz which were respectively assigned to immobile –CD_2– groups and to –CD_3– groups with rapid axial rotation. For samples at higher temperatures, motional averaging would likely lead to narrower ^{2}H patterns.

Figure 4a displays plots for each sample of the ^{13}CO regions of the S_0 and S_1 spectra for $\tau = 40$ ms. The strong signal at 178.7 ppm is dominated by the A11 ^{13}CO (~0.85 fraction) and Fig. 4b displays plots of $\Delta S/S_0$ vs τ for this signal. The peak shift is diagnostic of helical A11 (Zhang et al. 2003). The shoulder at 175.7 ppm is dominated by natural abundance lipid ^{13}CO nuclei and relative to the peptide signal, the lipid signal is less intense at longer τ which indicates a shorter lipid T_2. Comparison of lipid ^{13}C signals of the three samples (e.g.

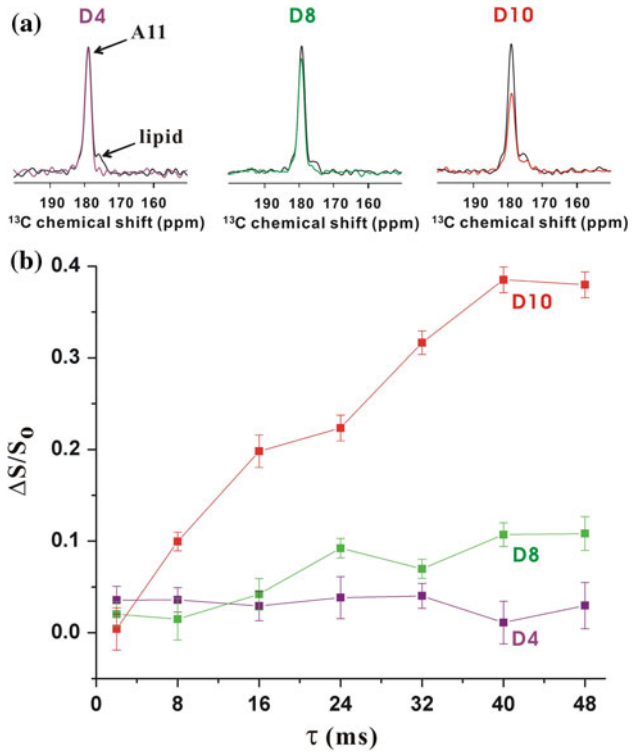

Fig. 4 KALP-A11$_C$ + D4, D8, or D10 membrane samples **a** $\tau = 40$ ms spectra and **b** plots of $\Delta S/S_0$ vs τ including $\pm \sigma$ uncertainties. Purple (D4), green (D8), and red (D10) match the Fig. 3 color pattern. The acquisition and processing parameters are similar to those used for I4-A9$_C$A8$_D$ and the $\Delta S/S_0$ analysis was based on 1.0 ppm integrations about the peak shift. The number of S_0 or S_1 scans varied between ~2000 for $\tau = 2$ ms and ~25000 for $\tau = 48$ ms

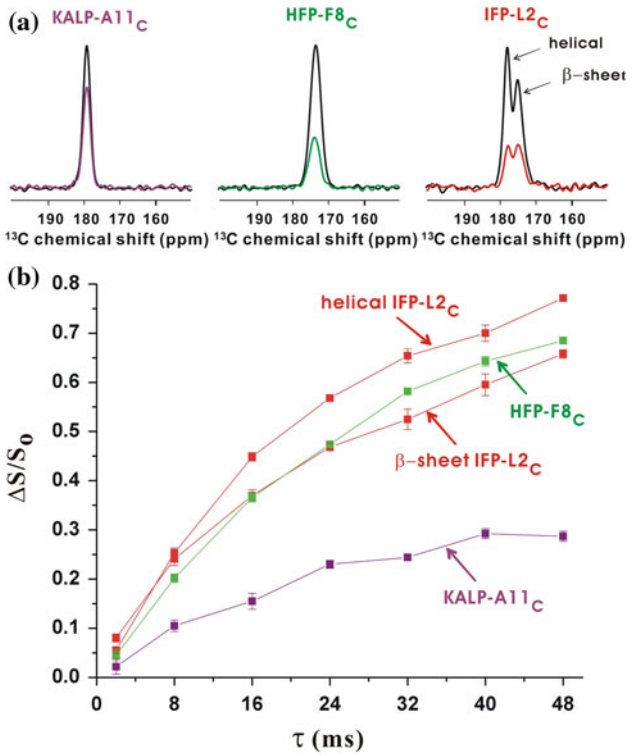

Fig. 5 Peptide + D54 membrane samples **a** $\tau = 40$ ms spectra and **b** plots of $\Delta S/S_0$ vs τ including $\pm \sigma$ uncertainties. The peptides are KALP-A11$_C$ (*purple*), HFP-F8$_C$ (*green*) and IFP-L2$_C$ (*red*). For IFP-L2$_C$, the different plots correspond to integration about the helical or β sheet peak shifts. For the KALP-A11$_C$ and HFP-F8$_C$ samples, the membrane molar composition was ditetradecylphosphatidylcholine (DTPC):ditetradecylphosphatidylglycerol (DTPG):D54:cholesterol (4:2:4:5) and for the IFP-L2$_C$ sample, the membrane composition was DTPC:DTPG:D54 (4:2:4). The DTPC, DTPG, and cholesterol lack carbonyl carbons. The sample, acquisition, processing, and $\Delta S/S_0$ analysis parameters are similar to those used for the KALP-A11$_C$ samples of Fig. 4

for $\tau = 2$ ms) shows the expected fastest dephasing of ^{13}CO in D4, $^{13}CD_3$ in D10, and $^{13}CH_2/^{13}CD_2$ in D8.

The Fig. 4 data are consistent with A11 ^{13}CO near the midpoint of the membrane, Fig. 3. The most rapid buildup and largest $\Delta S/S_0 \approx 0.4$ for $\tau = 40$ and 48 ms are observed with D10 whereas $\Delta S/S_0 \approx 0$ are observed with D4 for all τ. Intermediate $\Delta S/S_0 \approx 0.1$ are observed with D8 for $\tau = 40$ and 48 ms. The $\tau_{½} \approx 16$ ms with D10 is close to the $\tau_{½} \approx 20$ ms for I4-A9$_C$A8$_D$ and is consistent with similar ~5 Å ^{13}CO–^{2}H distances in both samples. The 5 Å distance for the D10 sample is also reasonable as the approximate sum of the Van der Waals radii of the helix and the ^{2}H atom. Relative to I4-A9$_C$A8$_D$, the lower asymptotic value of $\Delta S/S_0$ of D10 may be due to interference in the sum of the dipolar fields of multiple ^{2}H nuclei close to the A11 ^{13}CO. This idea is supported by similarity between the shape of the $\Delta S/S_0$ buildup of the D10 sample and the shape of the $\Delta S/S_0$ buildups from ^{13}CO–^{15}N REDOR of samples with ^{13}CO with multiple nearby ^{15}N nuclei (Balbach et al. 2000). Another potential reason for reduced $\Delta S/S_0$ is aggregation of KALP in the membrane. Relative to KALP monomers, labeled ^{13}CO nuclei on the interior of an aggregate would be more shielded from lipid acyl chains with consequent larger ^{13}CO–^{2}H distances and smaller ($\Delta S/S_0$). However, to our knowledge, there have been no reports of aggregation of transmembrane KALP. There are lysines at both ends of the KALP sequence and aggregation may be disfavored by intermolecular electrostatic repulsion.

Membrane location can also be probed in membranes with only a fraction of deuterated lipid. Figure 5 displays REDOR spectra and $\Delta S/S_0$ buildups for samples containing membranes with 0.4 lipid mol fraction D54 and either KALP-A11$_C$ or the HIV or influenza virus fusion peptides, HFP-F8$_C$ and IFP-L2$_C$ that are ^{13}CO labeled at F8 or L2, respectively. These peptides are N-terminal segments of viral proteins that aid catalysis of fusion between the virus and host cell membranes, likely through binding to the host cell membrane (Han and Tamm 2000; White et al. 2008; Pan et al. 2010). The HFP-F8$_C$ sequence is AVGIGALFLGFLG AAGSTMGARSWKKKKKKA and the IFP-L2$_C$ sequence

is GLFGAIAGFIENGWEGMIDGGGKKKKG (Han and Tamm 2000; Qiang et al. 2008). The incorporation of cholesterol in the membranes of the KALP-A11$_C$ and HFP-F8$_C$ samples was motivated by the significant fraction of cholesterol in the membranes of many cells including the host cells of HIV (Brugger et al. 2006). The peak shift of the HFP-F8$_C$ sample at 173.2 ppm is consistent with β sheet F8 structure whereas the peak shifts of the IFP-L2$_C$ sample at 177.6 and 174.7 ppm are consistent with populations of IFP molecules respectively with either helical or β sheet structure at L2 (Yang et al. 2002; Zhang et al. 2003; Qiang et al. 2008). For all peaks in the three samples there is substantial buildup of $\Delta S/S_0$ with $\tau_{½} \approx 16$ ms. For $\tau = 40$ or 48 ms, the $\Delta S/S_0$ is between ~ 0.3 and ~ 0.7. There are similar $\tau_{½}$s of the KALP-A11$_C$/D10 and the D54 samples as well as generally similar maximum $\Delta S/S_0$ values. For the D54 samples, these similarities support close contact of the labeled residue with the hydrophobic core of the membrane (Qiang et al. 2009). The different residues could have different locations within this core and the helical and β sheet IFP L2 could also have different locations.

Because the acyl chains of D54 are perdeuterated, a labeled peptide ^{13}CO nucleus may experience dipolar fields from multiple nearby ^{2}H nuclei. This may explain why $(\Delta S/S_0)^{max} > 2/3$ for the membrane-associated fusion peptide samples in Fig. 5. For two ^{2}H nuclei near the labeled ^{13}CO nucleus, there is 1/9 fractional probability that both ^{2}H nuclei are in the $m_s = 0$ state and would not undergo transitions during the π pulse. The ^{13}C/^{2}H/^{2}H spin triplets have $(\Delta S/S_0)^{max} \approx 8/9$ which is greater than the 2/3 value of ^{13}C/^{2}H spin pairs.

^{13}C–^{2}H REDOR should be generally applicable to determining membrane locations of peptides and proteins as well as the distributions of these locations. As shown in Fig. 4, greater insight may be obtained from comparison of $\Delta S/S_0$ between samples with different selectively deuterated lipids. Greater $\Delta S/S_0$ may be achievable with use of composite ^{2}H pulses. More extensive ^{13}C labeling including sidechain labeling may also be used assuming that there is adequate signal-to-noise for initial 2D ^{13}C–^{13}C correlation, adequate resolution in the 2D spectrum, and means to attenuate loss of signal from ^{13}C–^{13}C dipolar and J-couplings (Jaroniec et al. 1999; Schaefer 1999).

Acknowledgments The research was supported by NIH AI47153.

References

Balbach JJ, Ishii Y, Antzutkin ON, Leapman RD, Rizzo NW, Dyda F, Reed J, Tycko R (2000) Amyloid fibril formation by A$\beta_{16\text{-}22}$, a seven-residue fragment of the Alzheimer's β-amyloid peptide, and structural characterization by solid state NMR. Biochemistry 39:13748–13759

Brugger B, Glass B, Haberkant P, Leibrecht I, Wieland FT, Krasslich HG (2006) The HIV lipidome: a raft with an unusual composition. Proc Natl Acad Sci USA 103:2641–2646

Buffy JJ, Hong T, Yamaguchi S, Waring AJ, Lehrer RI, Hong M (2003) Solid-state NMR investigation of the depth of insertion of protegrin-1 in lipid bilayers using paramagnetic Mn^{2+}. Biophys J 85:2363–2373

Cady SD, Schmidt-Rohr K, Wang J, Soto CS, DeGrado WF, Hong M (2010) Structure of the amantadine binding site of influenza M2 proton channels in lipid bilayers. Nature 463:689–693

de Planque MRR, Goormaghtigh E, Greathouse DV, Koeppe RE, Kruijtzer JAW, Liskamp RMJ, de Kruijff B, Killian JA (2001) Sensitivity of single membrane-spanning alpha-helical peptides to hydrophobic mismatch with a lipid bilayer: effects on backbone structure, orientation, and extent of membrane incorporation. Biochemistry 40:5000–5010

Doherty T, Waring A, Hong M (2006) Membrane-bound conformation and topology of the antimicrobial peptide tachyplesin I by solid-state NMR. Biochemistry 45:13323–13330

Gallagher GJ, Hong M, Thompson LK (2004) Solid-state NMR spin diffusion for measurement of membrane-bound peptide structure: gramicidin A. Biochemistry 43:7899–7906

Gullion T (1998) Introduction to rotational-echo, double-resonance NMR. Concept Magn Reson 10:277–289

Gullion T (1999) A comparison between REDOR and θ-REDOR for measuring 13C–2D dipolar interactions in solids. J Magn Reson 139:402–407

Gullion T, Kishore R, Asakura T (2003) Determining dihedral angles and local structure in silk peptide by 13C–2H REDOR. J Am Chem Soc 125:7510–7511

Han X, Tamm LK (2000) A host-guest system to study structure-function relationships of membrane fusion peptides. Proc Natl Acad Sci USA 97:13097–13102

Hirsh DJ, Lazaro N, Wright LR, Boggs JM, McIntosh TJ, Schaefer J, Blazyk J (1998) A new monofluorinated phosphatidylcholine forms interdigitated bilayers. Biophys J 75:1858–1868

Huster D, Yao XL, Hong M (2002) Membrane protein topology probed by H-1 spin diffusion from lipids using solid-state NMR spectroscopy. J Am Chem Soc 124:874–883

Jaroniec CP, Tounge BA, Rienstra CM, Herzfeld J, Griffin RG (1999) Measurement of 13C–13–15 N distances in uniformly 13C labeled biomolecules: j-decoupled REDOR. J Am Chem Soc 121:10237–10238

Long HW, Tycko R (1998) Biopolymer conformational distributions from solid-state NMR: alpha-helix and 3(10)-helix contents of a helical peptide. J Am Chem Soc 120:7039–7048

McDermott A (2009) Structure and dynamics of membrane proteins by magic angle spinning solid-state NMR. Ann Rev Biophys 38:385–403

Pan JH, Lai CB, Scott WRP, Straus SK (2010) Synthetic fusion peptides of tick-borne encephalitis virus as models for membrane fusion. Biochemistry 49:287–296

Qiang W, Bodner ML, Weliky DP (2008) Solid-state NMR spectroscopy of human immunodeficiency virus fusion peptides associated with host-cell-like membranes: 2D correlation spectra and distance measurements support a fully extended conformation and models for specific antiparallel strand registries. J Am Chem Soc 130:5459–5471

Qiang W, Sun Y, Weliky DP (2009) A strong correlation between fusogenicity and membrane insertion depth of the HIV fusion peptide. Proc Natl Acad Sci USA 106:15314–15319

Sack I, Balazs YS, Rahimipour S, Vega S (2000) Solid-state NMR determination of peptide torsion angles: applications of ^{2}H-dephased REDOR. J Am Chem Soc 122:12263–12269

Schaefer J (1999) REDOR-determined distances from heterospins to clusters of ^{13}C labels. J Magn Reson 137:272–275

Schmidt A, McKay RA, Schaefer J (1992) Internuclear distance measurement between deuterium (I = 1) and a spin-1/2 nucleus in rotating solids. J Magn Reson 96:644–650

Toke O, Maloy WL, Kim SJ, Blazyk J, Schaefer J (2004) Secondary structure and lipid contact of a peptide antibiotic in phospholipid bilayers by REDOR. Biophys J 87:662–674

Tristram-Nagle S, Nagle JF (2004) Lipid bilayers: thermodynamics, structure, fluctuations, and interactions. Chem Phys Lipids 127: 3–14

White JM, Delos SE, Brecher M, Schornberg K (2008) Structures and mechanisms of viral membrane fusion proteins: multiple variations on a common theme. Crit Rev Biochem Mol Biol 43: 189–219

Yang J, Gabrys CM, Weliky DP (2001) Solid-state nuclear magnetic resonance evidence for an extended beta strand conformation of the membrane-bound HIV-1 fusion peptide. Biochemistry 40: 8126–8137

Yang J, Parkanzky PD, Bodner ML, Duskin CG, Weliky DP (2002) Application of REDOR subtraction for filtered MAS observation of labeled backbone carbons of membrane-bound fusion peptides. J Magn Reson 159:101–110

Zhang HY, Neal S, Wishart DS (2003) RefDB: a database of uniformly referenced protein chemical shifts. J Biomol NMR 25: 173–195

Zheng Z, Yang R, Bodner ML, Weliky DP (2006) Conformational flexibility and strand arrangements of the membrane-associated HIV fusion peptide trimer probed by solid-state NMR spectroscopy. Biochemistry 45:12960–12975